光学学报

微腔辅助的自旋动力学特性和超辐射相变

崔超，冯彦林*

山东师范大学物理与电子科学学院，光场调控及应用中心，山东 济南 250358

摘要 将玻色爱因斯坦凝聚制备在随时间简谐振荡的势场中，并与光学微腔系统相耦合，建立新的模型。分析了该模型中原子受到的有效磁场和简谐势阱的振动强度等因素对超辐射量子相变的影响，并探究了其随时间振荡的自旋动力学特性。提出的新模型具有重要的研究意义，且为深入研究腔量子调控提供了可行方案。

关键词 量子光学；光学微腔；超辐射；自旋动力学；玻色爱因斯坦凝聚

中图分类号 O469 **文献标志码** A **DOI**：10.3788/AOS231750

1 引 言

1924 年，爱因斯坦根据印度物理学家萨特延德拉·纳特·玻色提出的量子公式预言：玻色子体系中的绝大多数粒子会在温度接近绝对零度时聚集在能量最低的量子态上，在接近宏观的尺度上聚结为一个单一的量子力学实体，即可以用波函数描述的实体，称为玻色爱因斯坦凝聚（BEC）。然而由于技术和实验条件的限制，玻色爱因斯坦凝聚理论被提出后，很长一段时间里都未能在实验室中实现。直到 1995 年，麻省理工学院的埃里克·康奈尔和卡尔·威曼成功实现了稀薄原子气体的玻色爱因斯坦凝聚[1]，并因此获得了 2001 年的诺贝尔物理学奖，自此引发了相关研究热潮。如今，高度可操控的超冷原子物理已经成为物理学研究的一个热门方向，并引起了越来越多科学家们的关注[2-4]。例如，研究者们在超冷原子系统中预言并观测到了 Feshbach 共振，实现了光学晶格的构造以及自旋轨道耦合等[5-12]。超冷原子领域中最关键的是量子自旋系统，其不仅含有丰富的物理特性，而且具有广泛的应用前景。随着实验技术手段的不断发展，量子自旋系统已经在量子计算[13-16]、量子存储[17-20]和量子传感[21-22]等量子信息处理领域中有着重要的应用。因此，量子自旋系统的多体效应也成为目前物理学研究的热门方向之一。与传统的通过外加磁场来改变自旋自由度的方法相比，将原子自旋自由度和运动自由度相耦合的自旋轨道耦合方法是一种新的调控自旋方法。随着冷原子系统中的人工自旋轨道耦合在实验上不断实现，以自旋轨道耦合为基础的许多新奇物理现象的相关研究也得到了广泛的关注[23-26]。

另一方面，自 2010 年成功实现超辐射量子相变后[27]，超冷原子气体与腔量子电动力学相耦合的系统已经成为探索多体新奇物理的理想平台[28-36]，引发了科学家们的研究热潮。该耦合系统将超冷原子耦合到高精度的光学微腔中，在特定电磁边界条件下，使光与超冷原子发生相互作用并诱导出新奇的多体量子特性。在该耦合系统中，不仅可以探索以腔光子为媒介且被原子间无限长程相互作用所诱导的复杂量子行为[37-40]，还可以在单光子层次上认识并理解腔光子与超冷原子的集体动力学特性。同时，光学微腔既有驱动又有耗散，是一个天然的非平衡系统，因此可以研究其非平衡稳态动力学特性[41-42]。随着实验手段的不断发展，近期人们已经成功在超冷原子-光学微腔耦合系统中实现了人工自旋轨道耦合[43]。

本文将光学微腔系统与束缚于随时间振荡的简谐势阱中的玻色爱因斯坦凝聚相耦合，进一步实现和探索了在该振荡系统中影响超辐射量子相变的因素以及随时间振荡的自旋动力学特性。发现光与物质相互作用的耦合强度、原子受到的有效磁场和简谐势场的振动强度都会对相变产生不同程度的影响，而耦合强度和振动强度则跟光与原子相互作用所诱导的非平庸自旋动力学特性密切相关。

2 模型和平均场计算

2.1 模型和哈密顿量

当光场和原子耦合强度较弱时，光场和原子分别处于真空态和基态，系统处于正常态；而当两者耦合强度较强时，光场和原子的激发态被宏观占据，原子自发极化，系统处于超辐射态。因此，当增大光场和原子耦

收稿日期：2023-11-07；**修回日期**：2023-12-04；**录用日期**：2023-12-13；**网络首发日期**：2023-12-23

基金项目：国家自然科学基金（11947226，12004224）、中国博士后面上资助（2019M662421）

通信作者：*xiaogufyl89@163.com

合强度时，系统存在一个二阶的超辐射量子相变。由于超辐射相变要求光场和原子耦合强度与原子能级差相当，而原子能级差通常在光频率量级，比耦合强度高若干个数量级。对于真实的原子系统，原子的空间运动和超辐射相变会相互影响。值得注意的是，光学微腔内的玻色爱因斯坦凝聚会在外界横向驱动光场的作用下发生自组织现象，因此，利用光学微腔使得腔内的原子与光腔模式（光子）和横向驱动光相耦合，拉曼光子将两个不同的原子动量缀饰态耦合起来，有效的能级差与原子发射一个光子所获得的反冲能量相当，因而很容易获得相变的临界耦合强度，进而可以实现超辐射相变。

所提系统利用磁光阱制备玻色爱因斯坦凝聚，模型示意图如图 1 所示，将玻色爱因斯坦凝聚束缚于 yoz 平面内，同时在 x 方向存在随时间振荡的简谐势场，对应的简谐势场为 $V(x,t)=m\omega^2\left[x-x_0(t)\right]^2/2$，其中 m 为原子质量，ω 为束缚势场在 x 方向对应的频率，简谐势场中心 $x_0(t)$ 随时间 t 变化。原子在 t_0 时刻开始沿 x 方向进行简谐式周期振荡，该过程完全由 $x_0(t)$ 决定，为不失一般性，将 $x_0(t)$ 定义为高斯分布形式 $x_0(t)=\xi_0\exp\left[-(t-t_0)^2/\sigma_t^2\right]$，其中 ξ_0 和 σ_t 分别是峰值振幅（振动强度）和时间宽度[44-46]。将束缚于该振荡简谐势场中的玻色爱因斯坦凝聚耦合到高精度的光学微腔中，可以实现一个一维的耦合系统，且玻色爱因斯坦凝聚只沿 x 方向运动，腔模被沿 x 方向传播的线性极化激光所驱动，如图 1 横向箭头所示，图中磁场 B 方向垂直纸面向外。而玻色爱因斯坦凝聚由沿 y 方向传播的两束横向激光泵浦所产生，如图 1 纵向箭头所示。

所考虑的是主量子数为 5、能级层数为 2、轨道角动量量子数为 1、总角动量量子数为 3/2 的 ^{87}Rb，该原子是含有四个内态能级的玻色爱因斯坦凝聚，即两个简并的基态（$|\uparrow\rangle$ 和 $|\downarrow\rangle$）和两个激发态（$|1\rangle$ 和 $|2\rangle$），如图 2 所示。在塞曼场的作用下，基态分裂为两个与原基态能级能量相差均为 δ 的超精细基态。$|\downarrow\rangle\leftrightarrow|1\rangle$ 和 $|\uparrow\rangle\leftrightarrow|2\rangle$ 之间的跃迁（虚线箭头）是由耦合强度为 g 的量子化腔场引起的。$|\uparrow\rangle\leftrightarrow|1\rangle$ 和 $|\downarrow\rangle\leftrightarrow|2\rangle$ 跃迁（实线箭头）是由拉比频率为 Ω 的横向泵浦光引起的。玻色爱因斯坦凝聚与腔模和泵浦光相互作用产生两个独立的拉曼过程，使得两个自旋基态发生耦合，原子与泵浦光的拉比频率为 Ω，原子与腔模的耦合强度为 g，腔模频率 ω_c 与泵浦光的频率 ω_p 相接近，同时都远失谐于玻色原子的跃迁频率 ω_a，即失谐频率 $\Delta_a=\omega_p-\omega_a$，且满足 $|\Delta_a|\gg g,\Omega$。

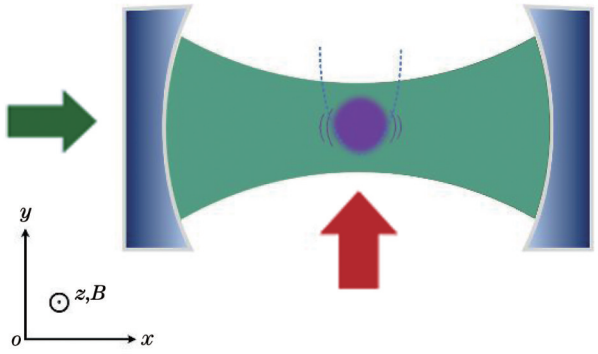

图 1　模型示意图

Fig. 1　Model diagram

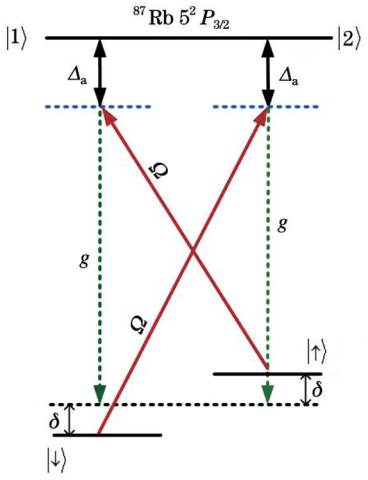

图 2　原子能级图及跃迁

Fig. 2　Atomic energy level diagram and transition

在上述大失谐的条件下，玻色爱因斯坦凝聚的激发态可以被绝热去除，因此考虑一个较深的简谐势阱（腔场的光学势阱忽略不计）并对原子自由度作二次量子化，系统的哈密顿量（约化普朗克常量 $\hbar=1$）可以表述为

$$\hat{H}=\sum_{\sigma=\uparrow,\downarrow}\int\hat{\psi}_\sigma^\dagger(x)\left\{\frac{\hat{p}_x^2}{2m}+\frac{1}{2}m\omega^2\left[x-x_0(t)\right]^2+\xi_\sigma m_z\right\}\hat{\psi}_\sigma(x)\mathrm{d}x-\Delta_C\hat{a}^\dagger\hat{a}+\eta\hat{a}^\dagger\left[\int\hat{\psi}_\downarrow^\dagger(x)\cos(k_0x)\hat{\psi}_\uparrow(x)\mathrm{d}x+\int\hat{\psi}_\uparrow^\dagger(x)\cos(k_0x)\hat{\psi}_\downarrow(x)\mathrm{d}x\right]+\mathrm{H.c.},\tag{1}$$

式中：$\hat{p}_x$ 为沿 x 方向动量的分量；$\xi_\sigma=\xi_\uparrow=-\xi_\downarrow=1$ 为不同自旋状态下对应的系数；H.c. 表示公式中前一项的复共轭；$m_z=\omega_\uparrow-\omega_\downarrow=2\delta$ 是超精细基态 $|\uparrow\rangle$ 和 $|\downarrow\rangle$ 能量劈裂，$\omega_\uparrow$ 和 $\omega_\downarrow$ 分别为两基态的特征频率；$\hat{a}^\dagger(\hat{a})$ 为光子的产生（湮灭）算符；$\eta=\Omega g/\Delta_a$ 为腔辅助拉曼过程的耦合强度；$\Delta_C=\omega_p-\omega_c$ 为腔场失谐；$\hat{\psi}_\sigma$ 为对应自旋状态下的玻色子场算符，$\hat{\psi}_\sigma$ 和 $\hat{\psi}_\sigma^\dagger$ 遵循玻色子对易关系；k_0 为泵浦的反冲动量。从式（1）中可以看出，光与物质相互作用使得原子内部自旋自由度与外部运动自由度相耦合，实现了自旋翻转。

2.2 平均场计算

给出腔场算符和玻色场算符的海森堡运动方程，同时对腔场自由度和原子场算符作平均场处理[47]，即$\langle\hat{a}\rangle\to\alpha$、$\hat{\boldsymbol{\psi}}_\sigma^\dagger(x)\to\psi_\sigma(x)$（场算符近似展开为凝聚态波函数），$\alpha$为光场序参量，$\psi_\sigma$为对应自旋状态下的波函数。由式(1)可得到如下的耦合平均场方程

$$\mathrm{i}\frac{\partial}{\partial t}\alpha=(-\Delta_{\mathrm{C}}-\mathrm{i}\kappa)\alpha+N\eta\theta, \tag{2}$$

$$\begin{cases}\mathrm{i}\dfrac{\partial}{\partial t}\psi_\uparrow(x,t)=\left\{\dfrac{\hat{p}_x^2}{2m}+\dfrac{m\omega^2}{2}\left[x-x_0(t)\right]^2+\xi_\uparrow m_z\right\}\psi_\uparrow(x,t)+2\mathrm{Re}\left\{\alpha(t)\right\}\eta(x)\psi_\downarrow(x,t)\\ \mathrm{i}\dfrac{\partial}{\partial t}\psi_\downarrow(x,t)=\left\{\dfrac{\hat{p}_x^2}{2m}+\dfrac{m\omega^2}{2}\left[x-x_0(t)\right]^2+\xi_\downarrow m_z\right\}\psi_\downarrow(x,t)+2\mathrm{Re}\left\{\alpha(t)\right\}\eta(x)\psi_\uparrow(x,t)\end{cases}, \tag{3}$$

式中：θ为原子自组织序密度，表示超辐射相变前后原子进入自组织相的序参量密度，$\theta=\int\theta(x)\mathrm{d}x=\int\cos(\boldsymbol{k}_0x)\left[\left\langle\psi_\uparrow^*(x)\psi_\downarrow(x)\right\rangle+\mathrm{H.c.}\right]\mathrm{d}x$，$\psi_\sigma^*$为$\psi_\sigma$的复共轭；$\eta(x)=\eta\cos(\boldsymbol{k}_0x)$体现了模态函数的空间依赖性；$\kappa$为腔场耗散率；$N$为原子数；i为虚数单位。可以看出式(3)为微腔辅助的凝聚态波函数的非线性薛定谔方程，即Gross-Pitaevskii (GP)方程。从式(2)、(3)可以看出，用$\alpha/\sqrt{N}$代替方程中的场振幅可以使参数缩放不影响最终计算结果，使得$\sqrt{N}\,\eta$保持恒定。也就是说，在平均场模型中，原子数可以合并到系统参数和场振幅变量中，因此在计算过程中，可以将$\sqrt{N}\,\eta$视为一个整体。

哈密顿量和GP方程均为含时方程，为方便求解，先对哈密顿量作幺正变换[23]

$$U=\exp\left[-\mathrm{i}m\omega^2F(t)\right], \tag{4}$$

式中：$F(t)=\int_0^t x_0(T)\mathrm{d}T=F_0\left\{f_{\mathrm{erf}}\left[(t-t_0)/\sigma_t\right]+f_{\mathrm{erf}}\left(t_0/\sigma_t\right)\right\}/2$。$x_0(T)$的表达式与$x_0(t)$相同，$T$仅为方便区分积分变量和积分上限引入，$F_0=\sqrt{\pi}\,\sigma_t\xi_0$，$f_{\mathrm{erf}}(x)$为误差函数，则式(1)可以写为

$$\begin{aligned}\hat{H}=&\sum_{\sigma=\uparrow,\downarrow}\int\hat{\boldsymbol{\psi}}_\sigma^\dagger(x)\left[\frac{\hat{p}_x^2}{2m}+\frac{1}{2}m\omega^2x^2+\omega^2F(t)\hat{p}_x+\xi_\sigma m_z\right]\hat{\boldsymbol{\psi}}_\sigma(x)\mathrm{d}x+\\&\eta\hat{a}^\dagger\left[\int\hat{\boldsymbol{\psi}}_\downarrow^\dagger(x)\cos(\boldsymbol{k}_0x)\hat{\boldsymbol{\psi}}_\uparrow(x)\mathrm{d}x+\int\hat{\boldsymbol{\psi}}_\uparrow^\dagger(x)\cos(\boldsymbol{k}_0x)\hat{\boldsymbol{\psi}}_\downarrow(x)\mathrm{d}x\right]+\mathrm{H.c.}-\Delta_{\mathrm{C}}\hat{a}^\dagger\hat{a}。\end{aligned} \tag{5}$$

假设时间宽度和振动强度分别满足$\sigma_t\to0$和$\xi_0\to\infty$，而$F_0=\sqrt{\pi}\,\sigma_t\xi_0$可以保持不变，在此条件下，$x_0(t)$可以视为一个Delta脉冲，可以将其表示为$F(t)=F_0\Theta(t-t_0)$，其中$\Theta(t-t_0)$是阶跃函数，因此，式(5)可以重新改写为

$$\hat{H}=\begin{cases}\displaystyle\sum_{\sigma=\uparrow,\downarrow}\int\hat{\boldsymbol{\psi}}_\sigma^\dagger(x)\left[\frac{\hat{p}_x^2}{2m}+\frac{1}{2}m\omega^2x^2+\xi_\sigma m_z\right]\hat{\boldsymbol{\psi}}_\sigma(x)\mathrm{d}x+\\ \eta\hat{a}^\dagger\left[\int\hat{\boldsymbol{\psi}}_\downarrow^\dagger(x)\cos(\boldsymbol{k}_0x)\hat{\boldsymbol{\psi}}_\uparrow(x)\mathrm{d}x+\int\hat{\boldsymbol{\psi}}_\uparrow^\dagger(x)\cos(\boldsymbol{k}_0x)\hat{\boldsymbol{\psi}}_\downarrow(x)\mathrm{d}x\right]+\mathrm{H.c.}-\Delta_{\mathrm{C}}\hat{a}^\dagger\hat{a}, & t<t_0\\ \displaystyle\sum_{\sigma=\uparrow,\downarrow}\int\hat{\boldsymbol{\psi}}_\sigma^\dagger(x)\left[\frac{\hat{p}_x^2}{2m}+\frac{1}{2}m\omega^2x^2+\omega^2F_0\hat{p}_x+\xi_\sigma m_z\right]\hat{\boldsymbol{\psi}}_\sigma(x)\mathrm{d}x+\\ \eta\hat{a}^\dagger\left[\int\hat{\boldsymbol{\psi}}_\downarrow^\dagger(x)\cos(\boldsymbol{k}_0x)\hat{\boldsymbol{\psi}}_\uparrow(x)\mathrm{d}x+\int\hat{\boldsymbol{\psi}}_\uparrow^\dagger(x)\cos(\boldsymbol{k}_0x)\hat{\boldsymbol{\psi}}_\downarrow(x)\mathrm{d}x\right]+\mathrm{H.c.}-\Delta_{\mathrm{C}}\hat{a}^\dagger\hat{a}, & t\geqslant t_0\end{cases}。 \tag{6}$$

从式(6)出发，可以重新得到不依赖于时间的GP方程，具体表达式为

$$\begin{cases}\mathrm{i}\dfrac{\partial}{\partial t}\psi_\uparrow(x,t)=\begin{cases}\left[\dfrac{\hat{p}_x^2}{2m}+\dfrac{1}{2}m\omega^2x^2+\xi_\uparrow m_z\right]\psi_\uparrow(x,t)+2\mathrm{Re}\left\{\alpha(t)\right\}\eta(x)\psi_\downarrow(x,t), & t<t_0\\ \left[\dfrac{\hat{p}_x^2}{2m}+\dfrac{1}{2}m\omega^2x^2+\omega^2F_0\hat{p}_x+\xi_\uparrow m_z\right]\psi_\uparrow(x,t)+2\mathrm{Re}\left\{\alpha(t)\right\}\eta(x)\psi_\downarrow(x,t), & t\geqslant t_0\end{cases}\\ \mathrm{i}\dfrac{\partial}{\partial t}\psi_\downarrow(x,t)=\begin{cases}\left[\dfrac{\hat{p}_x^2}{2m}+\dfrac{1}{2}m\omega^2x^2+\xi_\downarrow m_z\right]\psi_\downarrow(x,t)+2\mathrm{Re}\left\{\alpha(t)\right\}\eta(x)\psi_\uparrow(x,t), & t<t_0\\ \left[\dfrac{\hat{p}_x^2}{2m}+\dfrac{1}{2}m\omega^2x^2+\omega^2F_0\hat{p}_x+\xi_\downarrow m_z\right]\psi_\downarrow(x,t)+2\mathrm{Re}\left\{\alpha(t)\right\}\eta(x)\psi_\uparrow(x,t), & t\geqslant t_0\end{cases}\end{cases}。 \tag{7}$$

从式(6)和式(7)可以看出，可以将含时问题转化为不含时的分类讨论问题，从而对方程进行求解，进而研究系统的物理特性。

3　分析与讨论

3.1　稳态特性

基于对微腔-超冷原子耦合系统基本性质的理解，首先需要以 ω 为能量归一化单位、ω^{-1} 为时间归一化单位、$\sqrt{1/(m\omega)}$ 为长度归一化单位简化式(2)和式(7)。其次，分析系统的多体基态性质。由于在实验中存在腔场耗散，当腔场耗散很大的时候，$1/\kappa$ 远小于原子的运动自由度，此时腔场可以被绝热去除，即 $\partial\alpha/\partial t=0$，由式(2)可以得到对应的稳态腔场的具体形式

$$\alpha_0=\frac{N\eta\theta}{\Delta_C+\mathrm{i}\kappa}。\tag{8}$$

将式(8)代入式(7)中，通过数值计算得到凝聚态波函数，具体可利用虚时演化方法求解式(7)，即 $\tau=\mathrm{i}t$。反过来，将得到的凝聚态波函数代入式(8)中，可得到表征发生超辐射相变的自组织序密度 θ 随耦合强度的演化。如图 3 所示，当耦合强度 $\sqrt{N}\,\eta$ 达到某一临界值时，腔场会发生集体激发，即体系发生超辐射相变，相变的临界点 $\sqrt{N}\,\eta/\omega$ 约为 21.1。图 3 描绘了序密度随耦合强度变化的关系，简谐势阱的振动强度 $\xi_0/\sqrt{1/(\pi m\omega)}=25$，其中，相关参数：$\Delta_C/\omega=-400$、$\kappa/\omega=200$、$m_z/\omega=0.1$。值得注意的是，对于 $t<t_0$ 和 $t\geqslant t_0$ 两种情况，通过比较分析发现这两种情况下虽然发生超辐射相变的临界相变点不同，但趋势是相同的，所以只给出了 $t\geqslant t_0$ 时的基态特性。

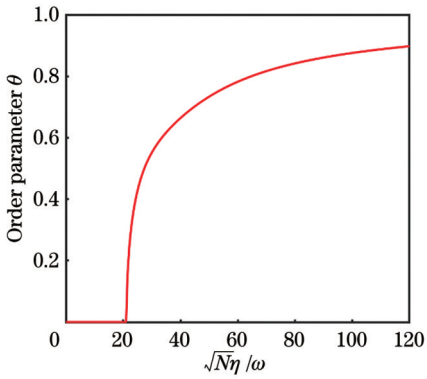

图 3　序密度 θ 随耦合强度变化的关系图

Fig. 3　Diagram of relationship between order parameter θ and coupling strength

除光与物质相互作用的耦合强度外，有效磁场强度 m_z 的大小也会对原子相变产生影响(磁场有无会相应地改变系统的对称性)。如图 4(a)所示，可以通过调节 m_z 的大小得到系统的稳态相图，系统存在两个相：正常(N)相和超辐射(SR)相，发生超辐射相变临界点所对应的耦合强度随着磁场强度 m_z 的增大而单调增大。

值得注意的是，简谐势阱的振动强度 ξ_0 也会影响原子相变，由于振动强度与原子的运动自由度相耦合，改变振动强度相应地改变原子的运动情况，因而在不同振动强度情况下，发生超辐射相变的临界点会随之改变。图 4(b)为 $\sqrt{N}\,\eta$-ξ_0 平面基态相图，在不同振动强度情况下，调节系统的耦合强度也可以实现从正常相到超辐射相的跃变。当 $\xi_0/\sqrt{1/(\pi m\omega)}\leqslant 31.5$ 时，发生超辐射相变的临界点所对应的耦合强度随振动强度的增大而减小；当 $\xi_0/\sqrt{1/(\pi m\omega)}>31.5$ 时，临界点所对应的耦合强度随振动强度的增大而增大。相关参数 $\Delta_C/\omega=-400$、$\kappa/\omega=200$，图 4(a)中 $\xi_0/\sqrt{1/(\pi m\omega)}=25$ 和图 4(b)中 $m_z/\omega=0.1$。

3.2　自旋动力学特性

在由数值自洽方法得到序参量 α_0 的基础上，为了描述有效光与原子相互作用所诱导的非平庸自旋动力学特性，需要选择一个能够描述该特性的物理量。基于光与物质相互作用使得玻色子自旋相反的两个内态发生耦合，两个自旋相反的轨道态是非正交的，因此，

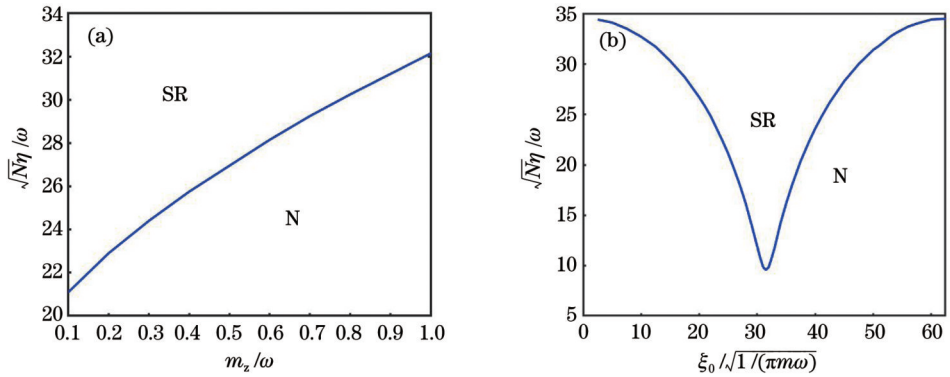

图 4　平面基态相图。(a) $\sqrt{N}\,\eta$-m_z 平面基态相图；(b) $\sqrt{N}\,\eta$-ξ_0 平面基态相图

Fig. 4　Plane ground state phase diagram. (a) Phase diagram of $\sqrt{N}\,\eta$-m_z plane ground state; (b) phase diagram of $\sqrt{N}\,\eta$-ξ_0 plane ground state

选择沿x方向的泡利算符$\sigma_x(t)$(两个自旋内态的混合)的平均值来分析自旋动力学特性。

当束缚势振动强度取一般值且体系未发生超辐射(耦合强度小),即自旋未发生耦合的情况时,$\langle\sigma_x(t)\rangle$随时间在零处对称振荡;而当体系发生超辐射(耦合强度大)时,$\langle\sigma_x(t)\rangle$随时间在零处的振荡对称性减弱且不再光滑,曲线不光滑意味着自旋已经发生耦合。图5(a)描绘了当束缚势振动强度$\xi_0\Big/\sqrt{1/(\pi m\omega)}=25$固定时,在耦合强度$\sqrt{N}\,\eta/\omega$分别为16.1(未发生超辐射)和26.1(发生超辐射)条件下,$\langle\sigma_x(t)\rangle$随$t\omega$变化的曲线。其他相关参数取值:$\Delta_C/\omega=-400$、$\kappa/\omega=200$、$m_z/\omega=0.1$。

除耦合强度外,振动强度$\xi_0\Big/\sqrt{1/(\pi m\omega)}$也会对$\langle\sigma_x(t)\rangle$产生影响。图5(b)为耦合强度$\sqrt{N}\,\eta/\omega=26.1$固定且其他参数不变时,振动强度$\xi_0\Big/\sqrt{1/(\pi m\omega)}=25$(实线)和$\xi_0\Big/\sqrt{1/(\pi m\omega)}=30$(虚线)对应的关系曲线图。当振动强度取特殊值且体系发生超辐射时,$\langle\sigma_x(t)\rangle$随时间的振荡是不对称的,对称性的破坏也就意味着自旋共振效应受束缚原子的振动势影响。由图4(b)可知,当$\xi_0\Big/\sqrt{1/(\pi m\omega)}\leqslant31.5$时,$\xi_0\Big/\sqrt{1/(\pi m\omega)}$增大会导致超辐射相变所对应的耦合强度减小。在这种情况下,增大$\xi_0\Big/\sqrt{1/(\pi m\omega)}$会同时增大系统的耦合强度与相变点对应耦合强度之差,可以理解为该状态下系统的"相对耦合强度"变大,系统的耦合变得更强。显然,可以预见的是,随着系统的耦合变强,耦合对系统的影响不断增大,$\langle\sigma_x(t)\rangle$的对称性将不断减弱且取值不断靠近1。

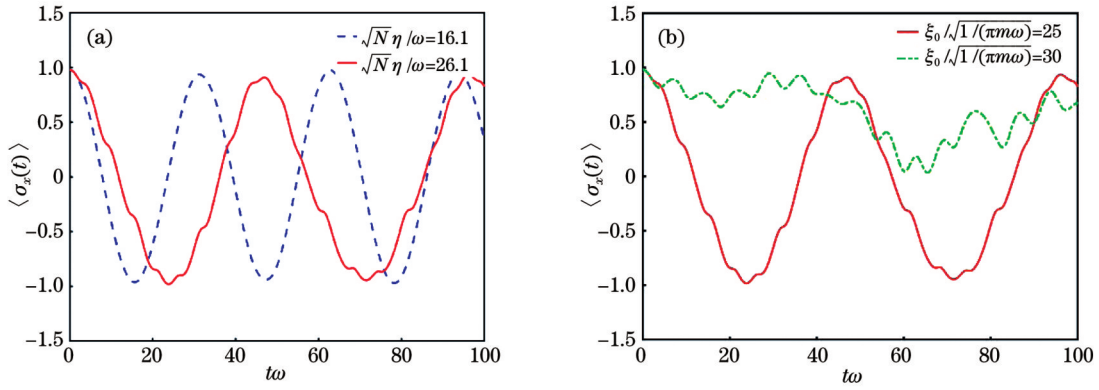

图5　$\langle\sigma_x(t)\rangle$随$t\omega$的变化曲线。(a)耦合强度对$\langle\sigma_x(t)\rangle$的影响;(b)振动强度对$\langle\sigma_x(t)\rangle$的影响

Fig. 5　Curves of $\langle\sigma_x(t)\rangle$ changing with $t\omega$. (a) Effect of coupling strength on $\langle\sigma_x(t)\rangle$; (b) effect of vibration intensity on $\langle\sigma_x(t)\rangle$

4　参数估计

本节估算所需参数同时表明在实验参数下可观测到相应的物理现象。具体地,选取的玻色爱因斯坦凝聚约为4.1×10^5个^{87}Rb原子,^{87}Rb原子的两个超精细内态可表示为$|F,m_F\rangle=|1,-1\rangle\equiv|\downarrow\rangle$和$|F,m_F\rangle=|2,-2\rangle\equiv|\uparrow\rangle$,其中$F$为总原子的总角动量,$m_F$为磁量子数。另一方面,选取波长为780 nm的法布里珀罗谐振腔作为高精度光学微腔,该谐振腔由两个曲率半径约为1 cm的曲面镜组成,忽略除基本TEM_{00}模式之外的所有腔模式,微腔的腰斑半径为35 μm,自由光谱范围大约为15 GHz,因此空腔精度$\sim5.5\times10^4$,束缚势场的频率$\omega\sim2\pi\times40$ Hz,通过对束缚谐振势施加梯度磁场可以实现随时振动的束缚势,振动的时间宽度$\sigma_t=0.05/\omega\approx0.2$ ms,其他参数的取值:$\kappa\sim50$ kHz、$\Delta_C\sim-130$ kHz、$m_z\sim25$ Hz。

当光子和原子都发生集体激发时,体系发生相应的超辐射相变。因此,可以通过光子的集体激发体现超辐射相变,光子数(漏出腔的光强变化)可以使用校准的单光子计数模块在腔外进行探测,通过调控拉比频率和单光子耦合强度,单光子计数模块可以对光强变化进行实时监测,从而可以得到序密度随耦合强度的变化图。另外,关于相图和自旋动力学特性的探测,可以通过玻色爱因斯坦凝聚的时间飞行吸收成像技术和漏出腔的光强变化来判定。因此,所提出的量子相、对应的量子相变以及自旋动力学特性能够在实验中被探测到。

5　结　　论

提出了一个可行的光学微腔辅助的超辐射相变和自旋动力学特性的实现方法并研究和探索了超辐射量子相变以及随时间振荡的非平庸自旋动力学特性。对腔场和物质场采用平均场近似的方法进行处理,并对含时系统进行处理得到系统的超辐射相变并给出了相变完整的相图,在此基础上,通过定性分析泡利算符的平均值来研究体系的非平庸自旋动力学特性。

参 考 文 献

[1] Anderson M H, Ensher J R, Matthews M R, et al. Observation of Bose-Einstein condensation in a dilute atomic vapor[J]. Science, 1995, 269(5221): 198-201.

[2] Davis K B, Mewes M O, Andrews M R, et al. Bose-Einstein condensation in a gas of sodium atoms[J]. Physical Review Letters, 1995, 75(22): 3969-3973.

[3] Lin Y J, Jiménez-García K, Spielman I B. Spin-orbit-coupled Bose-Einstein condensates[J]. Nature, 2011, 471(7336): 83-86.

[4] 热依扎·塔斯恒, 魏蔚, 周昱, 等. 平均场框架下两分量玻色-爱因斯坦凝聚中集体激发的阻尼[J]. 光学学报, 2023, 43(10): 1027002.
Reyza T, Wei W, Zhou Y, et al. Damping of collective excitations in two-component Bose-Einstein condensates using mean-field description[J]. Acta Optica Sinica, 2023, 43(10): 1027002.

[5] Wang P J, Yu Z Q, Fu Z K, et al. Spin-orbit coupled degenerate Fermi gases[J]. Physical Review Letters, 2012, 109(9): 095301.

[6] Galitski V, Spielman I B. Spin-orbit coupling in quantum gases [J]. Nature, 2013, 494(7435): 49-54.

[7] Hamner C, Qu C L, Zhang Y P, et al. Dicke-type phase transition in a spin-orbit-coupled Bose-Einstein condensate[J]. Nature Communications, 2014, 5: 4023.

[8] Mancini M, Pagano G, Cappellini G, et al. Observation of chiral edge states with neutral fermions in synthetic Hall ribbons [J]. Science, 2015, 349(6255): 1510-1513.

[9] Li J R, Huang W J, Shteynas B, et al. Spin-orbit coupling and spin textures in optical superlattices[J]. Physical Review Letters, 2016, 117(18): 185301.

[10] Livi L F, Cappellini G, Diem M, et al. Synthetic dimensions and spin-orbit coupling with an optical clock transition[J]. Physical Review Letters, 2016, 117(22): 220401.

[11] Song B, He C D, Zhang S C, et al. Spin-orbit-coupled two-electron Fermi gases of ytterbium atoms[J]. Physical Review A, 2016, 94(6): 061604.

[12] Kolkowitz S, Bromley S L, Bothwell T, et al. Spin-orbit-coupled fermions in an optical lattice clock[J]. Nature, 2017, 542(7639): 66-70.

[13] Loss D, DiVincenzo D P. Quantum computation with quantum dots[J]. Physical Review A, 1998, 57(1): 120-126.

[14] Hu X D, Das Sarma S. Spin-based quantum computation in multielectron quantum dots[J]. Physical Review A, 2001, 64(4): 042312.

[15] Wesenberg J H, Ardavan A, Briggs G A D, et al. Quantum computing with an electron spin ensemble[J]. Physical Review Letters, 2009, 103(7): 070502.

[16] Kloeffel C, Loss D. Prospects for spin-based quantum computing in quantum dots[J]. Annual Review of Condensed Matter Physics, 2013, 4: 51-81.

[17] Lvovsky A I, Sanders B C, Tittel W. Optical quantum memory [J]. Nature Photonics, 2009, 3: 706-714.

[18] Boehme C, McCamey D R. Nuclear-spin quantum memory poised to take the lead[J]. Science, 2012, 336(6086): 1239-1240.

[19] Julsgaard B, Grezes C, Bertet P, et al. Quantum memory for microwave photons in an inhomogeneously broadened spin ensemble[J]. Physical Review Letters, 2013, 110(25): 250503.

[20] Zaiser S, Rendler T, Jakobi I, et al. Enhancing quantum sensing sensitivity by a quantum memory[J]. Nature Communications, 2016, 7: 12279.

[21] Degen C L, Reinhard F, Cappellaro P. Quantum sensing[J]. Reviews of Modern Physics, 2017, 89(3): 035002.

[22] Poggiali F, Cappellaro P, Fabbri N. Optimal control for one-qubit quantum sensing[J]. Physical Review X, 2018, 8(2): 021059.

[23] Wu C H, Fan J T, Chen G, et al. Spin dynamics of a spin-orbit-coupled Bose-Einstein condensate in a Shaken harmonic trap[J]. Physical Review A, 2019, 99(1): 013617.

[24] 许文昊, 寿一畅, 罗海陆. 光的自旋-轨道相互作用[J]. 量子电子学报, 2022, 39(2): 159-181.
Xu W H, Shou Y C, Luo H L. Spin-orbit interaction of light[J]. Chinese Journal of Quantum Electronics, 2022, 39(2): 159-181.

[25] 黄帆, 贾信庭. 近场高阶庞加莱球上拉盖尔-高斯光束的自旋-轨道耦合[J]. 激光与光电子学进展, 2022, 59(7): 0726001.
Huang F, Jia X T. Spin-orbit coupling of Laguerre-gaussian beams on high-order Poincaré sphere in near field[J]. Laser & Optoelectronics Progress, 2022, 59(7): 0726001.

[26] 翟云佳, 陈园园, 张永平. 自旋轨道耦合诱导的调制不稳定性[J]. 光学学报, 2023, 43 (21): 2102001.
Zhai Y J, Chen Y Y, Zhang Y P. Spin-orbit-coupling-induced modulation instability[J]. Acta Optica Sinica, 2023, 43(21): 2102001.

[27] Baumann K, Guerlin C, Brennecke F, et al. Dicke quantum phase transition with a superfluid gas in an optical cavity[J]. Nature, 2010, 464(7293): 1301-1306.

[28] Wang C J, Gao C, Jian C M, et al. Spin-orbit coupled spinor Bose-Einstein condensates[J]. Physical Review Letters, 2010, 105(16): 160403.

[29] Fu Z K, Wang P J, Chai S J, et al. Bose-Einstein condensate in a light-induced vector gauge potential using 1064 nm optical-dipole-trap lasers[J]. Physical Review A, 2011, 84(4): 043609.

[30] Wu C J, Mondragon-Shem I, Zhou X F. Unconventional Bose-Einstein condensations from spin-orbit coupling[J]. Chinese Physics Letters, 2011, 28(9): 097102.

[31] Sinha S, Nath R, Santos L. Trapped two-dimensional condensates with synthetic spin-orbit coupling[J]. Physical Review Letters, 2011, 107(27): 270401.

[32] Hu H, Ramachandhran B, Pu H, et al. Spin-orbit coupled weakly interacting Bose-Einstein condensates in harmonic traps [J]. Physical Review Letters, 2012, 108(1): 010402.

[33] Zhang J Y, Ji S C, Chen Z, et al. Collective dipole oscillations of a spin-orbit coupled Bose-Einstein condensate[J]. Physical Review Letters, 2012, 109(11): 115301.

[34] Qu C L, Hamner C, Gong M, et al. Observation of Zitterbewegung in a spin-orbit-coupled Bose-Einstein condensate [J]. Physical Review A, 2013, 88(2): 021604.

[35] Olson A J, Wang S J, Niffenegger R J, et al. Tunable Landau-Zener transitions in a spin-orbit-coupled Bose-Einstein condensate[J]. Physical Review A, 2014, 90(1): 013616.

[36] Wu Z, Zhang L, Sun W, et al. Realization of two-dimensional spin-orbit coupling for Bose-Einstein condensates[J]. Science, 2016, 354(6308): 83-88.

[37] Landig R, Hruby L, Dogra N, et al. Quantum phases from competing short- and long-range interactions in an optical lattice [J]. Nature, 2016, 532(7600): 476-479.

[38] Léonard J, Morales A, Zupancic P, et al. Monitoring and manipulating Higgs and Goldstone modes in a supersolid quantum gas[J]. Science, 2017, 358(6369): 1415-1418.

[39] Léonard J, Morales A, Zupancic P, et al. Supersolid formation in a quantum gas breaking a continuous translational symmetry [J]. Nature, 2017, 543(7643): 87-90.

[40] Hruby L, Dogra N, Landini M, et al. Metastability and avalanche dynamics in strongly correlated gases with long-range interactions[J]. Proceedings of the National Academy of Sciences of the United States of America, 2018, 115(13): 3279-3284.

[41] 张莹, 陈梅雄, 李莹颖, 等. 光学微腔的应用和发展前景[J]. 激光与光电子学进展, 2015, 52(4): 040002.
Zhang Y, Chen M X, Li Y Y, et al. Application and development prospects of optical micro-resonators[J]. Laser & Optoelectronics Progress, 2015, 52(4): 040002.

[42] 张天才, 毋伟, 杨鹏飞, 等. 高精细度法布里-珀罗光学微腔及其在强耦合腔量子电动力学中的应用[J]. 光学学报, 2021, 41(1): 0127001.

Zhang T C, Wu W, Yang P F, et al. High-finesse micro-optical Fabry-Perot cavity and its applications in strongly coupled cavity quantum electrodynamics[J]. Acta Optica Sinica, 2021, 41(1): 0127001.
[43] Kroeze R M, Guo Y D, Lev B L. Dynamical spin-orbit coupling of a quantum gas[J]. Physical Review Letters, 2019, 123(16): 160404.
[44] Japha Y, Band Y B. Motion of a condensate in a shaken and vibrating harmonic trap[J]. Journal of Physics B: Atomic, Molecular and Optical Physics, 2002, 35(10): 2383-2389.
[45] Price H M, Ozawa T, Goldman N. Synthetic dimensions for cold atoms from shaking a harmonic trap[J]. Physical Review A, 2017, 95(2): 023607.
[46] Chen X, Jiang R L, Li J, et al. Inverse engineering for fast transport and spin control of spin-orbit-coupled Bose-Einstein condensates in moving harmonic traps[J]. Physical Review A, 2018, 97: 013631.
[47] Nagy D, Szirmai G, Domokos P. Self-organization of a Bose-Einstein condensate in an optical cavity[J]. The European Physical Journal D, 2008, 48(1): 127-137.

Microcavity-Assisted Spin Dynamics Characteristics and Superradiant Phase Transition

Cui Chao, Feng Yanlin*

Shandong Provincial Engineering and Technical Center of Light Manipulations, School of Physics and Electronics, Shandong Normal University, Jinan 250358, *Shandong, China*

Abstract

Objective Compared with the traditional method of changing spin freedom through external magnetic fields, the spin-orbit coupling, which utilizes the coupling between the spin freedom and the motion freedom of atoms, is a new method for regulating spin. With the continuous realization of artificial spin-orbit coupling in cold atomic systems in experiments, many novel physical phenomena based on spin-orbit coupling have been widely promoted. In addition, since the realization of the superradiant quantum phase transition in experiments in 2010, the system of coupling ultracold atomic gas and cavity quantum electrodynamics has become an ideal platform for exploring novel many-body physics, which has aroused a research boom among theoretical scientists and experimental scientists. This coupling system couples ultracold atoms into a high-precision optical microcavity. Under specific electromagnetic boundary conditions, light interacts with ultracold atoms and induces novel many-body quantum properties. In this coupling system, one can not only explore the complex quantum behavior induced by the long-range interaction among atoms mediated by cavity photons but also understand the collective dynamical properties of cavity photons and ultracold atoms at the single-photon level. At the same time, the optical microcavity has both driving and dissipation, and it is a natural non-equilibrium system, which allows one to study the non-equilibrium steady-state dynamical properties. However, the time-dependent cavity-assisted spin dynamics has not been considered experimentally and theoretically. On the one hand, the time-dependent Schrödinger equation is difficult to obtain an exact analytical solution mathematically, and on the other hand, the physical process expressed by the time-dependent Schrödinger equation involves complex energy changes, time evolution, and interaction problems, which makes it difficult to solve. In view of these problems, we proposed a method for realizing the superradiant phase transition with the assistance of an optical microcavity. This method coupled the optical microcavity system with a Bose-Einstein condensate trapped in a harmonic potential that oscillates with time to obtain a new model, which could be used to study the self-organized phase transition and spin dynamics of Bose-Einstein condensates in microcavities and provide a reference for studying other Bose-Einstein condensates based on spin.

Methods We considered the preparation of Bose-Einstein condensates using a magneto-optical trap and the coupling of these Bose-Einstein condensates bound in an oscillatory harmonic potential field with a high-precision optical microcavity, thereby establishing a one-dimensional coupled system where the Bose-Einstein condensates only moved in the x direction. The atoms we considered were those with four internal energy levels, and under conditions of large detuning, the excited states of the Bose-Einstein condensates were removed adiabatically, and the resulting Hamiltonian was then quantized. Through mean-field calculations, we obtained the coupled mean-field equations, which were then specialized for the time-dependent part, thereby transforming the problem with time dependence into a classification discussion without time dependence.

Results and Discussions We studied the steady-state properties of matter, obtained the relationship diagram of the order parameter with the coupling strength and explored the influence of the external magnetic field strength and the harmonic

potential field vibration strength on the critical point of the superradiant phase transition. The results show that the effective magnetic field m_z experienced by the atoms and the vibration strength ξ_0 of the harmonic potential well will affect the phase transition. Specifically, the coupling strength corresponding to the critical point of the superradiant phase transition increases monotonically with the increase in m_z. When $\xi_0 \Big/ \sqrt{1/(\pi m\omega)} \leqslant 31.5$, the coupling strength corresponding to the critical point of the superradiant phase transition decreases with the increase in ξ_0. When $\xi_0 \Big/ \sqrt{1/(\pi m\omega)} > 31.5$, the coupling strength corresponding to the critical point of the superradiant phase transition increases with the increase in ξ_0 (Fig. 4). In addition, we also analyzed the non-trivial spin dynamics induced by the interaction between light and atoms and the influence of the vibration strength of the harmonic potential field on the dynamical properties. It was found that when the system does not undergo superradiance, the oscillation of $\langle \sigma_x(t) \rangle$ at zero over time is still symmetric but not smooth, and the value of $\xi_0 \Big/ \sqrt{1/(\pi m\omega)}$ affects the atomic spin resonance effect (Fig. 5).

Conclusions In this study, we propose a feasible method for realizing optical microcavity-assisted superradiant phase transition and spin dynamics and explore the superradiant quantum phase transition and non-trivial spin dynamics that oscillate with time. We adopt the mean-field approximation method for the cavity field and the matter field and treat the time-dependent system, so as to obtain the superradiant phase transition of the system and give the complete phase diagram of the phase transition. On this basis, we study the non-trivial spin dynamics of the system by qualitatively analyzing the average value of the Pauli operator. We find that the coupling strength corresponding to the occurrence of the superradiant phase transition increases with the increase in the external magnetic field, and it decreases first and then increases with the increase in the vibration intensity of the external harmonic potential field. The vibration intensity of the harmonic potential field affects the spin dynamics effect of the system, because the vibration intensity of the harmonic potential field changes the coupling strength corresponding to the critical point of the superradiant phase transition, thus resulting in changes in the spin dynamics effect of the system.

Key words quantum optics; optical microcavity; superradiant; spin dynamics; Bose-Einstein condensate